

Experimental Investigation of Effect of Environment Temperature on Freeze-form Extrusion Fabrication

Xiyue Zhao¹, Michael S. Mason¹, Tieshu Huang¹, Ming C. Leu¹, Robert G. Landers¹, Gregory E. Hilmas², Samuel J. Easley³, Michael W. Hayes³

1870 Miner Circle

Department of Mechanical and Aerospace Engineering¹

Department of Materials Science and Engineering²

University of Missouri-Rolla, Rolla, Missouri 65409-0050

The Boeing Company, St. Louis, Missouri 63042³

{xzd2c, mmason, hts, mleu, landersr, ghilmas}@umr.edu

{Michael.w.hayes2, samuel.j.easle}@boeing.com

Reviewed, accepted September 4, 2007

Abstract

Freeze-form Extrusion Fabrication (FEF) is an additive manufacturing technique that extrudes ceramic loaded aqueous pastes layer by layer below the paste freezing temperature for component fabrication. A computer controlled 3-D gantry system has been developed for the FEF process. The system includes a temperature control subsystem that allows for fabrication of components below the paste freezing temperature. The low temperature environment allows for larger component fabrication. Comparisons in terms of layer thickness, self-sustaining ability, and system response were performed between 0 °C and -20 °C for alumina sample fabrications. The minimum deposition angles without use of support material have been determined for 20°C, 10 °C, 0 °C, -10 °C and -20 °C fabrications.

1. Introduction

Advanced ceramics are needed for applications in the aerospace, automotive and other industries [1]. Compared to conventional 3-D ceramic component fabrication techniques, which are costly and time-consuming because of mold preparation, Solid Freeform Fabrication (SFF) has the great potential of becoming an efficient and inexpensive manufacturing technique because it is a tool-less fabrication process. Recently more and more SFF techniques have been investigated and developed for ceramic processing. Well researched and commercialized SFF techniques for ceramic component fabrication include Fused Deposition of Ceramics (FDC) [2, 3], Stereolithography (SLA) [4], 3-D printing (3DP) [5, 6], and Selective Laser Sintering (SLS) [7, 8]. In the FDC process, the ceramic-thermoplastic material is heated into a semi-liquid state and extruded through a nozzle. The extruded material is deposited on an X-Y working surface in a layer-by-layer fashion. The solids loading is typically 40-50 vol.%. FDC uses a high percentage of organic chemical binders at 40-50 vol.% [3]. Stereolithography of ceramic components is implemented by mixing resins with ceramic particles which can be polymerized when exposed to ultraviolet light. However, the laser scattering at the ceramic particles reduces the cure depth and widens the cured area, thus reducing the dimension accuracy [4]. 3-D printing of ceramic components includes two approaches according to applied materials: hot-melt dry powder and aqueous based pastes. The dry powder method is similar to 3-D printing where the binder is selectively printed onto the powder bed [5]. The main concern of this method is the relatively low green density, only up to 35 vol. %. In recent years aqueous based ceramic pastes

were explored to overcome this problem [6]. Selective Laser Sintering was applied in ceramic part fabrication by mixing organic binder (typically PMMA) with ceramic particles as the process material [7], but the post-sintering density is relatively low at about 55% [8].

Most SFF techniques for ceramic component fabrication involve the use of organic binders. In some processes, such as FDC, the binder content may be as high as 40 to 50 vol.%. This organic binder needs to be removed during post processing and generates harmful wastes that are undesirable for the environment [9]. Freeze-form Extrusion Fabrication (FEF) extended the idea of the rapid freeze prototyping (RFP) method [10-13], where water droplets are deposited on demand and freeze on a 2-D motion substrate for the fabrication of 3D components in a layer-by-layer manner. FEF uses an aqueous ceramic paste with a solids loading up to 50 vol.%. The organic binder content is only 2-4 vol. %. In FEF, aqueous-based ceramic paste is extruded using a ram extruder and deposited on a 2-D motion substrate. After the deposition of each layer the Z-axis moves up by one layer thickness and the next layer is deposited. This process is repeated until the component is completely fabricated. Freeze-drying is used to prevent crack formation during the drying process. After freeze-drying, the binder is removed in a rapid heating cycle because of the low binder content. Finally, the parts are sintered at 1550 °C. The post processing has been detailed previously [9]. FEF has some unique advantages, such as large component fabrication, high density of sintered components, low percentage of organic binder, and almost no material waste. FEF is an environmentally friendly SFF technique.

In the present paper, a custom-deigned 3D gantry system with a custom-designed cooling system (0 °C to -30 °C) was used for FEF processing. The layer thickness optimization was performed for fabrication at -20 °C. The self-sustaining ability of the process at different temperatures was analyzed. The time constant and gain of the first-order process model of FEF were calculated. The trends of these two parameters during fabrication at -20 °C and at 0 °C were recorded and analyzed.

2. Experimental Setup and Procedure

2.1 Experimental setup

The 3-D gantry system, as shown in Figure 1, consists of three orthogonal linear axes from Velmex BiSlide (Velmex, Bloomfield, NY), each with a 508 *mm* travel range. The X-axis consists of two parallel slides and is used as the support for the Y-axis. The two parallel slides provide smooth and stable motion and allow more fabrication space. The Z-axis is mounted on the Y-axis and the extrusion mechanism is mounted on the Z-axis. All axes are mounted with limit switches on both ends. Four DC motors (Pacific Scientific PMA22B), each with a resolver for position feedback at a resolution of 1000 counts per revolution drive the axes. Each motion axis has a maximum speed of 127 *mm/s* and a resolution of 0.00254 *mm*. All the axes are controlled by a Delta-Tau Turbo PMAC PCI board.

The right image in Figure 1 shows an enlarged view of the extrusion mechanism. It is a ram extruder driven by a DC motor (Kollmorgen AKM23D), which has an encoder with a resolution of 0.254 μm and is mounted on the Z-axis slide. An Omega LC305-1KA load cell (Danaher Motion, Wood Dale, IL) is mounted between the plunger and the ram extruder to

measure the extrusion force. An analog-to-digital conversion board (Delta-Tau ACC28) converts the analog signal from the load cell to digital signal and inputs to the PMAC board.

The 3-D gantry is located inside a freezer. A condenser is used to keep the freezer temperature at $0\text{ }^{\circ}\text{C}$ ($\pm 2\text{ }^{\circ}\text{C}$). Liquid nitrogen is used for lowering the temperature of the freezer between $0\text{ }^{\circ}\text{C}$ to $-30\text{ }^{\circ}\text{C}$. A temperature controller (Omega CN132) (Danaher Motion, Wood Dale, IL) is used to control the temperature of the freezer through a solenoid valve, which regulates the flow rate of nitrogen. As shown in Figure 2, two heating coils are installed around the extruder and the nozzle to keep the paste temperature in the range of $10\text{-}15\text{ }^{\circ}\text{C}$ to prevent the paste from freezing.

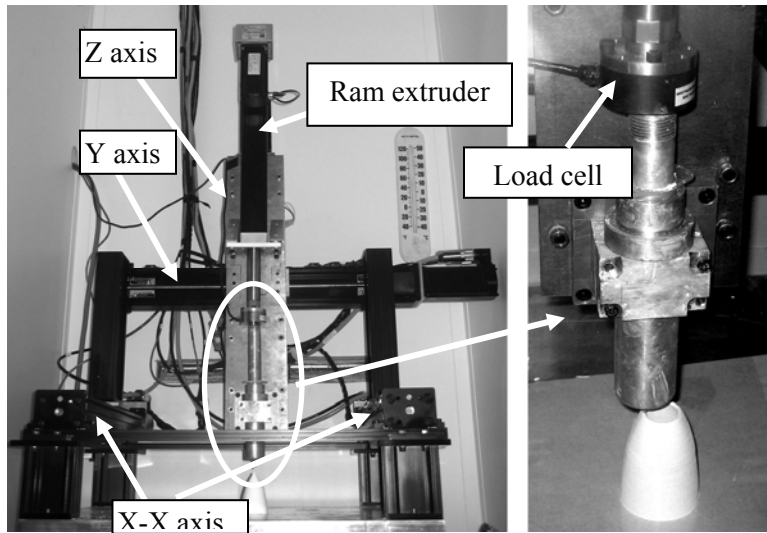


Figure 1: The 3D gantry system with extrusion mechanism.

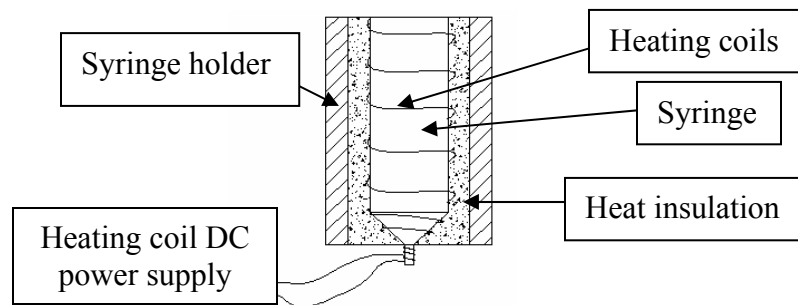


Figure 2: Schematic drawing showing the syringe and nozzle heating system.

2.2 Process parameters

The process parameters include initial extrusion force, extrusion force increment, road offset, layer thickness, and X-Y motion table (working surface) speed. The road offset between deposition trajectories was mainly determined by the diameter of the nozzle. A $580\text{ }\mu\text{m}$ diameter nozzle was used in all experiments. The X-Y motion speed was in a range of $10\text{-}20\text{ mm/s}$. The X-

Y table speed was set at a certain speed and the layer thickness was adjusted according to nozzle size and fabrication temperature.

A larger extrusion force is associated with a higher extrusion rate. The initial extrusion force was set to 311 *N*. To maintain a constant extrusion rate and avoid nozzle clogging, the reference extrusion force was continually increased slowly. An adaptive PI controller was designed and implemented to control the ram velocity in a range of $\pm 50 \mu\text{m/s}$ at steady state to achieve the desired extrusion.

2.3 Investigation of fabrication at different temperatures

2.3.1 Layer thickness effect

The layer thickness determined by the Z-axis shift distance needs to be carefully adjusted, so that the nozzle does not disturb the previous layer during the deposition process. To optimize this parameter, cylinder samples were fabricated at 0 °C and -20 °C with different layer thicknesses and X-Y table speeds as listed in Table 1. The table speed for fabrication at -20 °C was slightly larger than at 0 °C to compensate for the temperature effect of the paste.

Table 1: Deposition parameters used in the layer thickness experiments

	Temperature (°C)	X-Y table speed (mm/s)	Layer thickness (μm)
1	0	10	510
2	-20	11	510
3	-20	11	580
4	-20	11	640

2.3.2 Minimum deposit angle test

The minimum deposit angle is the minimum angle that can be achieved between the substrate and the slope of a hollow cone without collapse. This angle reflects the offset ability of the FEF process in building a 3-D part without use of support material. Three sets of tests were conducted to fabricate cones with different bottom diameters to find the minimum deposit angle. The tested temperatures include 20 °C, 10 °C, 0 °C, -10 °C, and -20 °C. In each set of tests, hollow cones were fabricated using bottom diameters of 38 *mm*, 51 *mm*, and 64 *mm*. The cone height was varied to determine the lowest height without collapse of the cone during the building process for calculation of the minimum deposit angle.

2.3.3 Time constant and gain

The FEF process contains many nonlinear effects, such as air bubbles trapped within the paste, uneven water content in different portions of the paste, various sizes of agglomerates, etc. Paste consistency is also slightly different from batch to batch. These factors contribute to difficulties in modeling the paste extrusion process. Previous research work shows that the

extrusion process, in general, can be approximated as a first-order dynamic system, where commanded voltage to the ram motor amplifier is the input and extrusion force is the output [10]. However, according to the experimental data, there is significant variation in the model parameters during the extrusion. Therefore, the Recursive Least Square (RLS) method is applied to model the extrusion process and to determine how the amount of remaining paste in the material reservoir affects the dynamic model parameters. The model input is the commanded ram motor voltage, which is processed by a 16 bit digital-to-analog converter before going into the ram motor amplifier. The output is the measured extrusion force, which is sent to the computer via an analog-to-digital converter. The resolution of the measured extrusion force is 2.224 N.

Experiments were conducted to investigate how the parameters of the extrusion dynamic model varied during extrusion. In these experiments, a command ram motor voltage of 3 mV is sent to the motor amplifier for 10 seconds, and then the voltage is changed to -1.5 mV for 5 seconds, increased to 3.75 mV for another 10 seconds, and decreased to -1.75 mV for 5 seconds. Each test lasted until approximately 5 ml of paste was extruded. The extrusion force was measured with a sample period of 0.06 sec, and the RLS method was applied to estimate the model parameters at each sample period. The experiments were repeated at two environment temperatures.

3. Results and Discussion

3.1 Relationship between extrusion force and extrusion rate

During fabrication the extrusion rate decreased as the amount of paste in the syringe decreased when the extrusion force was constant. The table speed was maintained constant during fabrication. Therefore, the decrease in extrusion rate may result in under-filling and generating scraps in the building area as shown in Figure 3. Although the reason for this phenomenon is still not entirely clear, it is believed that this phenomenon is related to the paste property changing during the extrusion. There is a redistribution of liquid phase versus solid phase in the paste as the extrusion process proceeds.

The extrusion force should be gradually increased to balance the gradual increase of the paste resistance force during extrusion. The optimal rate of extrusion force increase during fabrication was approximately 2.3×10^{-2} N/s. By using an adaptive PI controller at a sample period of 0.06 seconds, the extrusion force followed the continually increasing reference force closely as shown in Figure 4.

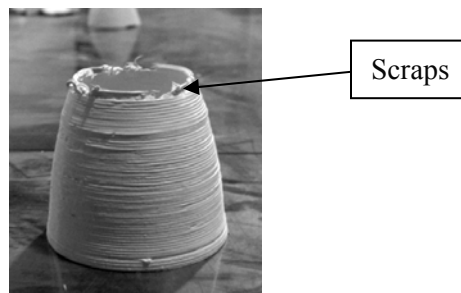


Figure 3: Picture showing scraps on a tangent ogive hollow cone.

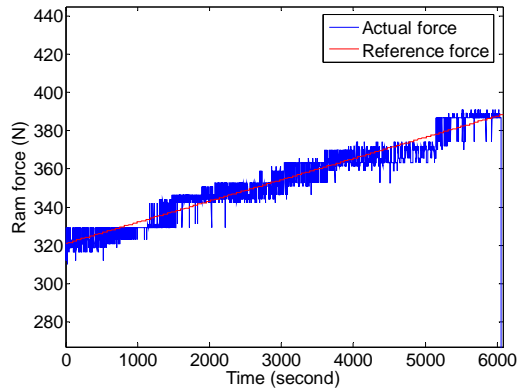


Figure 4: Reference force vs. actual ram force during an extrusion process.

3.2 Temperature effects

At 20 °C environment temperature, the extruded material drying rate was found to be fairly high if the moisture was less than 60%. The high drying rate was usually associated with non-uniform drying, which generated cracks and caused warping in the fabricated part. Increasing moisture in the surrounding area could help in improving sample quality.

At 0 °C, water evaporated more slowly and the drying rate is much lower than that at 20 °C. The surface finish of the samples fabricated at this temperature was generally smoother than the surface finish of those fabricated at 20 °C.

Because the extruded materials dried slowly and didn't freeze, the lower portion of the component did not have enough strength to support the whole component toward the end of the fabrication for a large component. This may lead to component deformation or even collapse. Decreasing the table speed ($< 12.5 \text{ mm/s}$), which increases drying time, could help solve this problem. However, the slow deposition rate would increase the fabrication time, which is undesirable.

At -20 °C, heating coils (Figure 2) were used to keep the paste warm at 10-15 °C to ensure proper extrusion. The extruded ceramic paste could freeze at -20 °C. No visible part deformation was observed. The table speed used for fabrication at -20 °C was 15-20 mm/s , while 10-12 mm/s was used for fabrication at 0 °C. Table 2 shows a general comparison of fabrication at these three temperatures.

Table 2: Results of layer thickness experiments

Environment Temperature (°C)	Dry Rate	Freeze Rate	Table Speed (mm/s)	Part Deformation	Part Surface
-20	Low	High	15-20	No	Smooth
0	Medium	None	10-12	Yes	Smooth
20	High, non-uniform	None	10-12	Yes	Cracks and warping

3.3 Comparison of part fabrication at different temperatures

3.3.1 Layer thickness effect

Five cylinders were fabricated for each layer thickness. Figure 5 shows one typical cylinder for each value listed in Table 1. Cylinder 1 was fabricated at 0 °C, while cylinders 2-4 were fabricated at -20 °C. Visually cylinder 1 has the best surface finish. This is because at this temperature, the extruded paste had a high viscosity ($>50 Pa \cdot s$). As a result, the new layer of material deforms slightly, making the surface smoother. The layer thickness for this fabrication was 510 μm , which was slightly less than the diameter of the nozzle (580 μm). At -20 °C, the paste froze quickly and exhibited little deformation. When using the same layer thickness (510 μm), the surface quality was poor as shown in Figure 5 (cylinder 2). This is because the paste material did not deform and the nozzle tip scratched the previously deposited materials. By increasing the layer thickness to 580 μm , the cylinder (Figure 5, cylinder 3) had a better surface finish. When the layer thickness was increased to 640 μm , the cylinder (Figure 5, cylinder 4) had an even better surface finish. However, when the layer thickness was larger than 640 μm , under-filling occurred. Therefore, the optimal layer thickness should be 640 μm for fabrication at -20 °C.

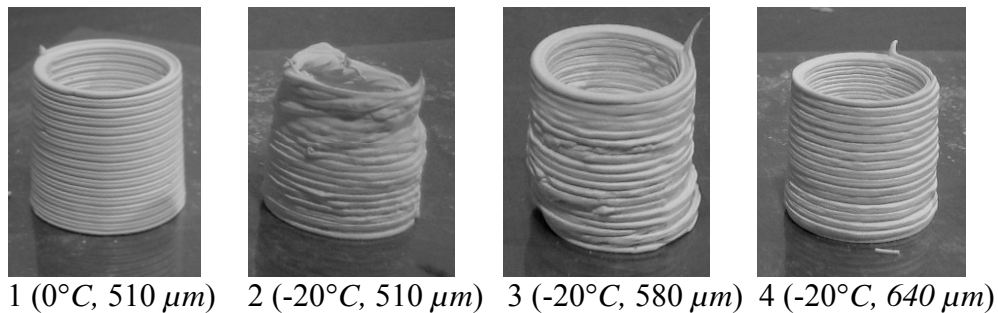


Figure 5: Cylinders fabricated using the parameters in Table 1

3.3.2 Minimum deposit angle test

Figure 6 gives the definition of the minimum deposit angle. Figure 7 shows a successfully built cone with 19 mm height and a 38 mm bottom diameter (left) and a collapsed cone (right).

The minimum deposit angle test results are given in Table 3. The relationships between the minimum deposit angle and the fabrication temperature are plotted in Figure 8. The figure shows that the minimum deposit angle increases quickly from -20 °C to 0 °C, then more slowly from 0 °C to 10 °C, and the trend further flattens from 10 °C to 20 °C. In the -20 °C experiment, the extruded materials froze and became solid quickly. This is the reason for the smallest minimum deposit angle at this temperature for the range between -20 °C and 20 °C. When the temperature increased to 0 °C, the extruded materials would not freeze but the viscosity was high. As the temperature increased, the viscosity became lower and the minimum deposit angle increased.

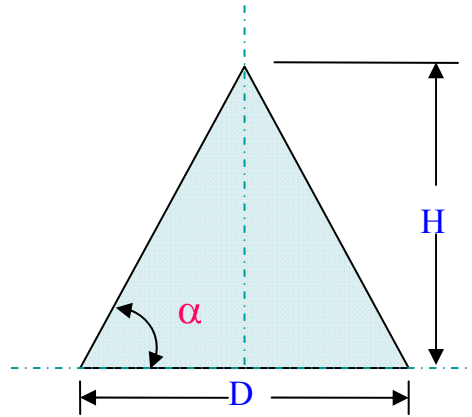


Figure 6: Definition of the minimum deposit angle.

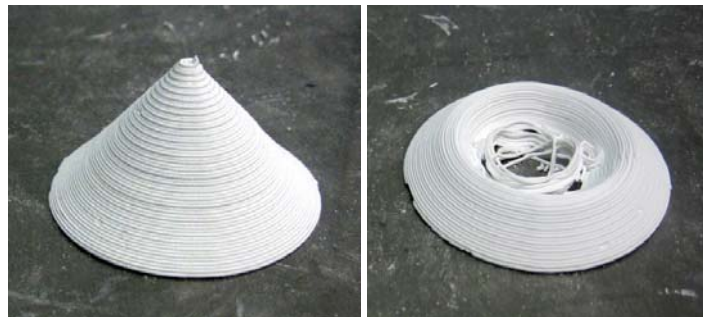


Figure 7: A successfully built cone (left) and a collapsed cone (right)

Table 3: Minimum deposit angle test results

Fabrication Temperature (°C)	Bottom Diameter = 38 (mm)	Bottom Diameter = 51 (mm)	Bottom Diameter = 64 (mm)
	Minimum deposit angle (°)	Minimum deposit angle (°)	Minimum deposit angle (°)
-20	27.47	25.64	23.75
-10	34.22	34.61	34.53
0	37.72	41.35	43.35
10	38.66	45.58	49.04
20	40.91	47.73	50.57

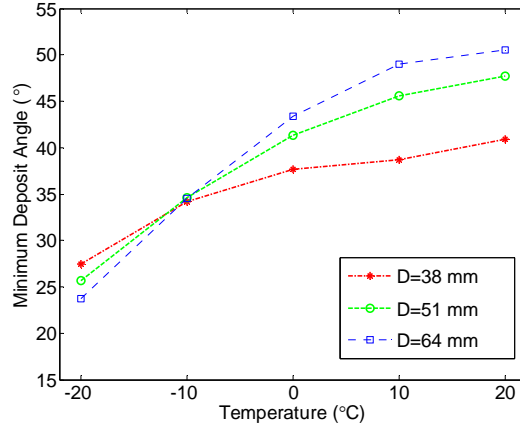


Figure 8: Minimum deposit angle as a function of temperature for different bottom diameters.

3.3.3 Time constant and gain

It has been shown that the dynamics of the extrusion process can be modeled by a first-order process [14]. In this section, the effect of environment temperature on the model parameters is explored. The transfer function of the first-order process in the digital domain is

$$G(z) = \frac{F(z)}{V(z)} = \frac{K(1-a)}{z-a} \quad (1)$$

where z is the forward shift operator, F is the ram force (N), and V is the DC voltage sent to the ram motor amplifier. The difference equation corresponding to equation (1) is

$$F(k) = aF(k-1) + K[1-a]V(k-1) = \boldsymbol{\eta}\boldsymbol{\phi} \quad (2)$$

where k is the iteration number. The unknown parameter vector and the regression variable vector, respectively, are

$$\boldsymbol{\eta} = [a \quad K(1-a)] = [a \quad b] \quad (4)$$

$$\boldsymbol{\phi} = [F(k-1) \quad V(k-1)]^T \quad (5)$$

In this form, the Recursive Least Squares technique can be applied to the experimental data to estimate the parameters a and b . The model parameters (i.e., time constant τ and gain K) are derived from the estimated parameters a and b and, respectively, are

$$\tau = -\frac{T}{\ln a} \quad (6)$$

$$K = \frac{b}{1-a} \quad (7)$$

Table 4 shows the model time constants and gains for six experiments at 0°C and six experiments at -20°C. The model time constants and gains for each experiment were calculated by taking the average of the last 100 data points of the total data gathered in each experiment. The data is graphed in Figure 9. The model time constant and the gain of model at -20°C showed the same trend as those at 0°C: the time constant decreased and the gain increased as the initial volume of paste in the reservoir decreased. This is because as the paste is extruded, air bubbles leave and liquid migration occurs causing the paste to become drier and stiffer. The model time constant in each experiment at -20°C was smaller than the corresponding time constant at 0°C, and the model gain at -20°C was lower than the corresponding model gain at 0°C. The reason for this is that the paste temperature used in the -20 °C experiment was increased 10~15°C by the heater; therefore, the paste temperature was higher than that of the paste in the 0°C experiment. The higher paste temperature in the -20°C experiment made the paste thinner and, thus, easier to extrude than the paste in the 0 °C experiment.

Table 4: The time constant and gain of FEF at -20 °C and 0 °C

Test	Volume of remaining paste (ml)	FEF at -20 °C		FEF at 0 °C	
		Time constant (s)	Gain (N/mV)	Time constant (s)	Gain (N/mV)
1	35	108.03	761.38	117.79	794.66
2	30	95.58	825.51	110.36	881.46
3	25	85.47	889.93	103.52	920.43
4	20	75.72	931.06	91.27	935.82
5	15	65.28	936.75	87.69	980.16
6	10	40.32	973.61	61.43	1035.18

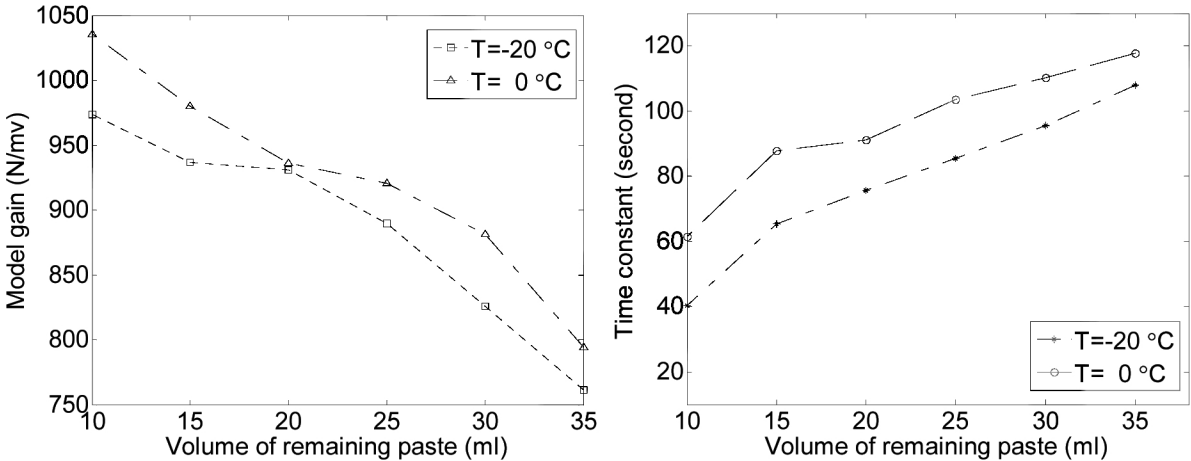


Figure 9: Trends of Model gains and time constants at -20 °C and 0 °C

3.4 Demonstration of components fabrication

Figure 10 shows tangent ogive cones in green state fabricated by the FEF process at $-20\text{ }^{\circ}\text{C}$ environment temperature. The left image shows a cone made from alumina paste and the right image shows two cones made from zirconium diboride.

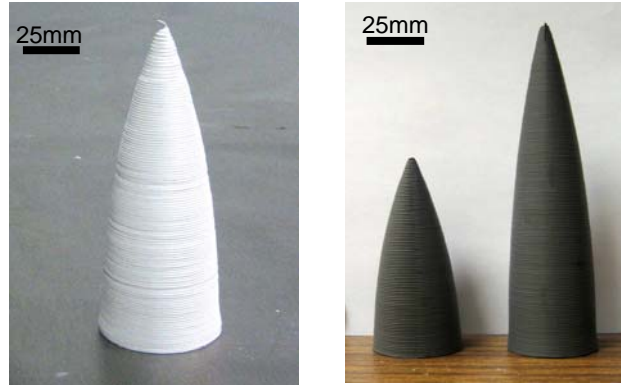


Figure 10: One Al_2O_3 and two ZrB_2 tangent ogive hollow cones in green state

4. Summary and Conclusions

The environment temperature has been found to significantly affect the material extrusion and deformation behavior in the freeze-from extrusion fabrication (FEF) process using aqueous-based ceramic pastes. Fabricating samples at $-20\text{ }^{\circ}\text{C}$ allows the deposited paste to freeze during the fabrication process. This results in the lowest minimum deposit angle, which means the highest self-sustaining ability (without the use of support material). The minimum deposit angle is strongly related to the environment temperature. The lower the environmental temperature is, the smaller the minimum deposit angle will be. Thus the FEF process can fabricate larger parts at $-20\text{ }^{\circ}\text{C}$ than at $0\text{ }^{\circ}\text{C}$. By using a heater to prevent the paste from freezing, the model time constant and the model gain are both smaller at $-20\text{ }^{\circ}\text{C}$ than the values of these parameters at $0\text{ }^{\circ}\text{C}$. Therefore, at $-20\text{ }^{\circ}\text{C}$, the paste with heating is easier to extrude, and the system response is faster than at $0\text{ }^{\circ}\text{C}$ without heating the paste. The successful fabrication of tangent ogive cones at $-20\text{ }^{\circ}\text{C}$ from alumina and zirconium diboride pastes have demonstrated the feasibility of the FEF process.

Acknowledgement

This work was supported by the Air Force Research Laboratory under Contract FA8650-04-C-5704.

References

1. T. S. Huang, "Fabrication of Ceramic Components Using Freeze-form Extrusion Fabrication," *Ph.D. Dissertation*, Department of Materials Science and Engineering, University of Missouri-Rolla (2007).

2. G. M. Lous, I. A. Cornejo, T. F. McNlty, A. Safari, and S. C. Danforth, "Fabrication of Piezoelectric Ceramic/Polymer Composite Transducers Using Fused Deposition of Ceramics," *J. Am. Ceram. Soc.*, **83** [1] 124-28 (2000).
3. J. J. McIntosh, S. C. Danforth and V. R. Jamalabad, "Shrinkage and Deformation in Parts Manufactured by Fused Deposition of Ceramics," *Proceedings of the Solid Freeform Fabrication Symposium*, Austin, Texas, August 11-13, 159-166 (1997).
4. T. Himmer, T. Nakagawa and H. Noguchi, "Stereolithography of Ceramics," *Proceedings of the Solid Freeform Fabrication Symposium*, Austin, Texas, August 11-13, 363-369 (1997).
5. E. M. Sachs, M. J. Cima, J. Brecht, and A. Curodeau, "CAD-Casting: The Direct Fabrication of Ceramic Shells and Cores by Three Dimensional Printing," *Man. Rev.*, **5** [2] 117-126 (1992).
6. J. Grau, J. Moon, S. Uhland, M. Cima and E. Sachs, "High Green Density Ceramic Parts Fabricated by the Slurry-Based 3DP process," *Proceedings of the Solid Freeform Fabrication Symposium*, Austin, Texas, August 11-13, 371-378 (1997).
7. J. P. Kruth, P. Mercelis, L. Froyen, and M. Rombouts, "Binding Mechanisms in Selective Laser Sintering and Selective Laser Melting" *Rapid Prototyping Journal*, **11**[1]26-36 (2005).
8. P. K. Subramanian, J. W. Barlow and H.L. Marcus, "Effect of Particle Size on SLS and Post-Processing of Alumina with Polymer Binders," *Proceedings of the Solid Freeform Fabrication Symposium*, Austin, Texas, August 7-9, 346-352 (1995).
9. T. S. Huang, M. S. Mason, G. E. Hilmas, and M. C. Leu, "Freeze-form Extrusion Fabrication of Ceramics," *Journal of Virtual and Physical Prototyping*, **1** [2], 93-100 (2006).
10. G. Sui, "Modeling and Analysis of Rapid Freeze Prototyping," *PhD Dissertation*, University of Missouri-Rolla, Rolla, Missouri (2002).
11. F. Bryant, G. Sui, and M. C. Leu, "A Study on the Effects of Process Parameters in Rapid Freeze Prototyping," *Proceedings of Solid Freeform Fabrication Symposium*, Austin, Texas, August 5-7, 635-642 (2002).
12. M. C. Leu, W. Zhang, and G. Sui, "An Experimental and Analytical Study of Ice Part Fabrication with Rapid Freeze Prototyping," *Annals of the CIRP*, **49** [1], 147-150 (2000).
13. G. Sui, and M. C. Leu, "Investigation of Layer Thickness and Surface Roughness in Rapid Freeze Prototyping," *ASME Journal of Manufacturing Science Engineering*, **125** [3], 555-563 (2002).
14. M.S. Mason, T. Huang, R. G. Landers, M. C. Leu, and G. E. Hilmas, "Freeform Extrusion of High Solids Loading Ceramic Slurries, Part I: Extrusion Process Modeling," *Proceedings of Solid Freeform Fabrication Symposium*, Austin, Texas, August 17-19 (2006).